Composite Structures 337 (2024) 118031

Contents lists available at ScienceDirect

Composite Structures

journal homepage: www.elsevier.com/locate/compstruct

A mesoscale computational approach to predict ABD matrix of thin woven composites

Hao Jin [a], Ning An [b,c,*], Qilong Jia [d], Xiaofei Ma [e], Jinxiong Zhou [f,**]

[a] School of Mechanical Engineering, Hangzhou Dianzi University, Hangzhou 310018, People's Republic of China
[b] School of Aeronautics and Astronautics, Sichuan University, Chengdu 610065, People's Republic of China
[c] State Key Laboratory of Structural Analysis for Industrial Equipment, Dalian University of Technology, Dalian 116024, People's Republic of China
[d] Shanghai Jeatron Technology Co., Ltd, Shanghai 201800, People's Republic of China
[e] Xi'an Institute of Space Radio Technology, Xi'an 710100, People's Republic of China
[f] State Key Laboratory for Strength and Vibration of Mechanical Structures and School of Aerospace, Xi'an Jiaotong University, Xi'an 710049, People's Republic of China

ARTICLE INFO

Dataset link: https://github.com/XJTU-Zhou-group/ABAQUS-Plugin-of-ABD-matrix

Keywords:
ABD matrix
Woven composites
RVE homogenization
Finite element method

ABSTRACT

The ABD matrix is a fundamental method to characterize the overall stiffness behavior of laminated composite structures. Although classical laminate theory has been widely used, it has limitations in predicting the ABD matrix for woven composites. To address this issue, this paper presents a mesoscale homogenization approach aimed at computing the ABD matrix for thin woven composites accurately. The mesoscale representative volume element (RVE) of the woven composite is generated using TexGen and imposed with periodic boundary conditions to enforce the Kirchhoff thin plate assumption. The ABD matrix is computed by conducting six separate finite element simulations, each representing one simple in-plane or out-of-plane deformation in a specified direction. Moreover, to facilitate the implementation of the method, an open-source plugin tool was developed within ABAQUS CAE, automating the ABD matrix calculation for various types of woven composites including 2D weave, 3D weave, and multiaxial. The accuracy of the proposed method was validated through benchmark calculations against existing literature results.

1. Introduction

Composite materials have gained increasing popularity in various high-performance structural designs including aerospace, automotive, and civil engineering components, due to their remarkable mechanical properties such as high specific stiffness and strength [1,2]. Unidirectional laminates and woven composites are two commonly used types of fiber-reinforced composites, each with its own characteristics and advantages. Unidirectional laminates consist of multiple layers with each layer having all fibers oriented in the same orientation and embedded in a matrix material. Woven composites, on the other hand, are composed of fiber yarns interlaced in a crisscross pattern, creating a woven-like structure with fibers oriented in multiple directions. Woven composites offer several advantages compared to unidirectional laminates, including enhanced mechanical isotropy, improved impact resistance, and superior damage tolerance. However, these benefits come with tradeoffs, such as increased manufacturing complexity and higher cost. The modeling of the stiffness behavior of woven composites is also a quite more complicated task compared to unidirectional laminates.

The ABD matrix is a fundamental concept in classical laminate theory (CLT) to characterize the effective stiffness properties of composite laminates, which relates the strains (ε_x, ε_y, γ_{xy}) and curvatures (κ_x, κ_y, κ_{xy}) in the midplane of the laminate to the resultant forces (N_x, N_y, N_{xy}) and moments (M_x, M_y, M_{xy}) exerted on the laminate. The constitutive equation is given as follows:

$$\begin{pmatrix} N_x \\ N_y \\ N_{xy} \\ M_x \\ M_y \\ M_{xy} \end{pmatrix} = \begin{pmatrix} A_{11} & A_{12} & A_{16} & B_{11} & B_{12} & B_{16} \\ A_{12} & A_{22} & A_{26} & B_{12} & B_{22} & B_{26} \\ A_{16} & A_{26} & A_{66} & B_{16} & B_{26} & B_{66} \\ B_{11} & B_{12} & B_{16} & D_{11} & D_{12} & D_{16} \\ B_{12} & B_{22} & B_{26} & D_{12} & D_{22} & D_{26} \\ B_{16} & B_{26} & B_{66} & D_{16} & D_{26} & D_{66} \end{pmatrix} \cdot \begin{pmatrix} \varepsilon_x \\ \varepsilon_y \\ \gamma_{xy} \\ \kappa_x \\ \kappa_y \\ \kappa_{xy} \end{pmatrix} \quad (1)$$

* Corresponding author at: School of Aeronautics and Astronautics, Sichuan University, Chengdu 610065, People's Republic of China.
** Corresponding author.
E-mail addresses: anning@scu.edu.cn (N. An), jxzhouxx@mail.xjtu.edu.cn (J. Zhou).

https://doi.org/10.1016/j.compstruct.2024.118031
Received 16 August 2023; Received in revised form 24 November 2023; Accepted 12 March 2024
Available online 16 March 2024

where the sub-matrices $[A]$ and $[D]$ represent the in-plane extensional and out-of-plane bending stiffness properties of the laminate, respectively, and $[B]$ represents the coupling between the in-plane and out-of-plane loads and deformations. The ABD matrix provides valuable insights into the deformation behaviors of a laminate under any complex load conditions. It serves as a vital concept in the design and analysis of composite laminated structures, and hence the accurate calculation of the ABD matrix is crucial for analyzing any complex behaviors of composite laminated structures.

CLT provides an effective analytical approach for determining the ABD matrix of composite laminates made up of multiple layers of unidirectional laminas. It is assumed that each unidirectional lamina within the laminate is homogeneous and exhibits mechanical orthotropy, and the laminate is composed of multiple laminas that are oriented according to a predetermined stacking sequence. Each entry in the ABD matrix is derived as a function of the mechanical properties of the unidirectional lamina, the thickness of the laminate, and the prescribed stacking sequence of fiber orientations [3]. CLT can also be employed to analyze the effective properties for woven composites. Zhang et al. [4] and Dang et al. [5–7] proposed an equivalent lamina element method to predict the in-plane stiffness, strength, and progressive damage of various types of woven composites. Their approach involved dividing a unit cell of the woven composite into several subcells and representing each subcell with equivalent unidirectional laminates. This conversion allowed the use of CLT to derive analytical solutions of effective properties for woven composites. However, the existing analytical solutions are limited to calculating the in-plane effective properties of woven composites. Other researches have demonstrated that the out-of-plane bending stiffness properties predicted by CLT are far from experimental measurements for woven composites [8–14]. For example, Soykasap [14] carried out experiments on thin laminates composed of plain weave woven composites and reported a considerable discrepancy of up to 400% in the bending stiffness when compared the experimental results to the predictions made by CLT.

On the other hand, finite element (FE)-based homogenization approach offers an alternative numerical method for computing the ABD matrix of woven composite. A mesoscale representative volume element (RVE) of a woven composite typically comprises the structural arrangement of yarns or fibers, along with their interactions and the surrounding matrix materials. Researchers developed homemade programs to address the specific complex heterogeneity associated with woven composites, allowing for accurate predictions of the laminate's overall mechanical properties [15,16]. Kueh and Pellegrino [17] developed a homogenized Kirchhoff plate approach to model the linear elastic response of single-ply triaxial weave fabric composites. The ABD matrix for the plate was computed by using the standard finite element method with mesoscale RVE analysis, and the numerical results were validated against experiments. Mallikarachchi [18] extended the method to predict the ABD matrix for two-ply plain weave laminates and examined the effect of different idealization of cross-sectional and weave profiles using five different tow models and demonstrated that the relative positioning of plies influences both extensional and bending stiffness of the laminate. Gao et al. [19] applied a similar multiscale strategy to predict the ABD matrix of 1/3 broken twill weave composite laminates. The numerical predictions were validated with experimental results and demonstrated a significant effect of the asymmetric weave architecture on the tensile stiffness of the laminates. In addition to the RVE approach, another homogenization approach proposed by Yu et al. [20] is the mechanics of structural genome (MSG) method. Under this theory, the minimal mathematical unit for constructing macro structures is named the structural genome (SG), which breaks the limitation of full periodicity required by the general RVE model, enabling the unified construction of constitutive models for multiscale structures including 3D constructs, beams, plates, and shells. A notable advantage of MSG is the bidirectional communication that facilitates between micro and macro structures: the SG model provides constitutive relations for predicting macro responses, and the responses at specific locations of the structure can be fed back to the SG model to observe local fields within the microstructure [21–23]. These methods provide valuable insights for efficiently and accurately predicting the equivalent stiffness, strength, and failure behaviors of woven composites, and with special processing, they can be used to obtain the ABD matrix of the woven composites [24].

The modeling strategy for predicting the ABD matrix for woven composites can be summarized as a two-step multiscale homogenization method [25,26], as depicted in Fig. 1. The first step involves creating a microscale RVE that represents the microstructure of the composite yarns. This step determines the effective material properties of the composite yarns through homogenization of the fiber and matrix properties in the yarn microstructure. The second step utilizes the obtained yarn properties to analyze the behavior of the woven composite by considering a mesoscale RVE, which homogenizes the yarn and matrix properties in the mesostructure of the woven composite and yields the ABD matrix as a result. By implementing this two-step homogenization approach into the standard finite element method, researchers are able to predict the ABD matrix of woven composites with improved accuracy. It is worth noting that the first step of microscale RVE homogenization, which involves estimating the effective orthotropic properties of the yarn, is the same as estimating the properties of a continuous fiber-reinforced unidirectional lamina. In this regard, a few user-defined programs and plugin tools have been developed to simplify the pre-and post-processing of micro-RVE analysis within commercial FE packages [27–29]. Among them, we developed the ABAQUS plugin named *Viscoelastic RVE Calculator* which provides an easy-to-use and robust way to evaluate both the elastic and viscoelastic mechanical properties of the fiber-reinforced unidirectional lamina in a previous study [29]. The implementation of periodic boundary conditions is crucial in FE-RVE analysis. It is important to note that the specific requirements for periodic boundary conditions can differ between micro-RVE and meso-RVE [30]. The micro-RVE focuses on capturing the interactions between individual fibers and the matrix under six in-plane specific loading conditions, which include three axial loadings and three shear loadings [see the left panel in Fig. 1]. In contrast, the meso-RVE takes a larger-scale perspective and considers the arrangement of multiple yarns and their interlacing pattern in woven composites. It aims to capture the overall deformation of the woven composite when it is subjected to not only in-plane extensional loads but also out-of-plane bending moments [see the middle panel in Fig. 1]. The calculation results of the micro-RVE analysis are the engineering constants of the composite yarn, while the result yielded by the meso-RVE analysis is the ABD matrix for the woven composite. The ABD matrix can finally be used to define the constitutive behavior of woven composites in the standard finite element analysis, facilitating deformation analysis of any thin-walled composite laminates [see the right panel in Fig. 1].

This study presents a mesoscale computational approach aimed at determining the ABD matrix for a range of woven composite types. Utilizing the Kirchhoff thin plate assumption and applying derived periodic boundary conditions, the approach computes each entry of the ABD matrix by considering the deformation of the RVE under six distinct loading conditions—three in-plane and three out-of-plane cases. Furthermore, the proposed approach has been implemented into an ABAQUS plugin to streamline and automate the calculation process. By making the source code publicly available to the community, we anticipate that our efforts will contribute to offering a robust and user-friendly approach for calculating the ABD matrix of woven composite laminates. We also note that the method developed here, along with our previously developed microscale RVE analysis approach and plugin *Viscoelastic RVE Calculator* [29], provides an integrated multiscale approach to predict the overall stiffness behavior of thin woven composite laminated structures.

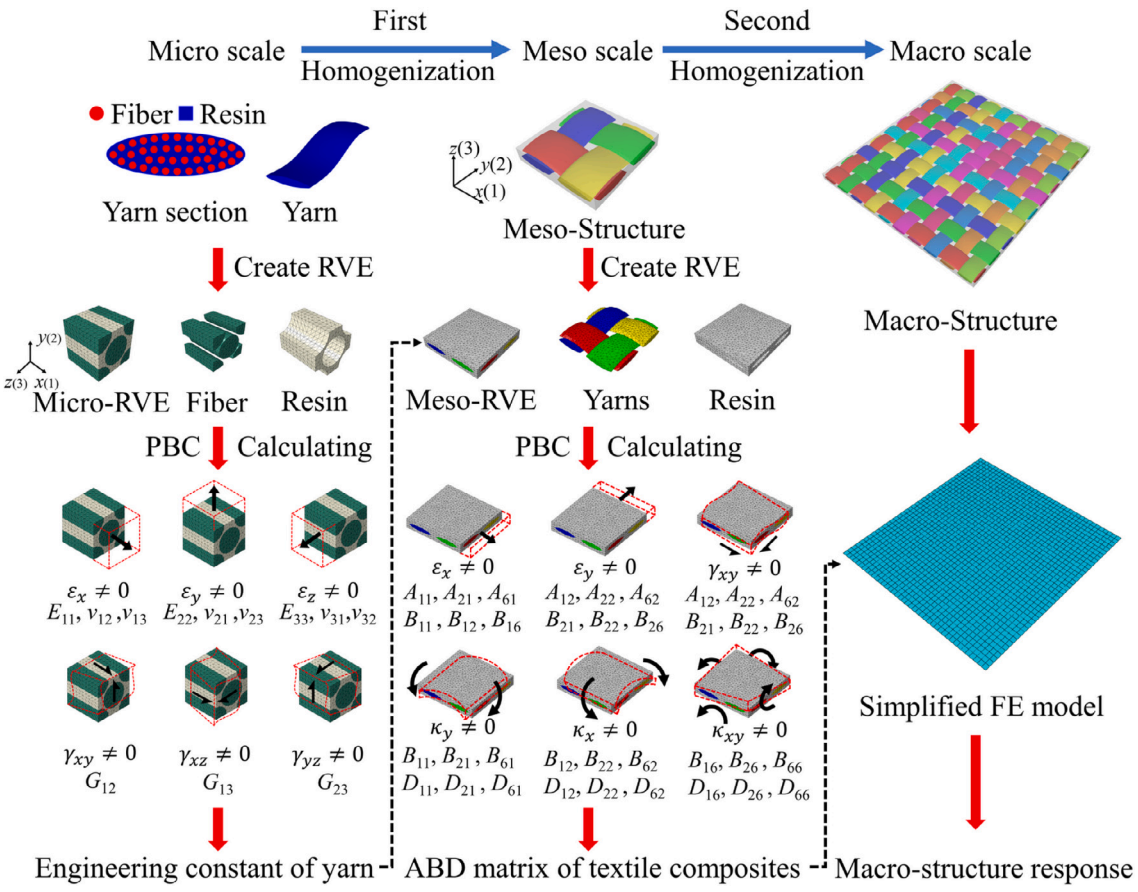

Fig. 1. Modeling framework of the two-step multiscale homogenization method for predicting the ABD matrix of woven composites.

The rest of the content is organized as follows: Section 2 describes the Kirchhoff plate homogenization approach, which involves the construction of mesoscale RVE models, the implementation of periodic boundary conditions, and the application of loading conditions; Section 3 provides a detailed description of the computation framework and functionalities of AMWC; In Section 4, the accuracy and validity of AMWC are demonstrated through several numerical examples including 2D weave composites, 3D woven composites, and multiaxial weave composites; and finally, Section 5 concludes with discussions and conclusions.

2. Mesoscale RVE homogenization approach

2.1. Construction of mesoscale RVE

An optimal mesoscale RVE of the woven composite shall be the smallest portion of the material that captures the essential mesoscale structural characteristics such as the weave pattern, cross-section of the yarn, undulation path of the yarn, matrix regions, interfaces, and any other relevant features. It is essential to precisely capture the weave pattern of the woven composite and the cross-sectional shape of the yarn in order to generate an accurate mesoscale RVE model. This is typically achieved using optical microscopy techniques [18,19]. Fig. 2 shows the construction of a mesoscale RVE for a two-ply plain weave laminate as an example. The cross-section of the laminate was examined by a Nikon optical microscope [18], and then the obtained optical micrograph was imported into AutoCAD software to measure the dimensions of the RVE, the cross-sectional shape of the yarn, and the interlacing path of the yarns. The overall geometry of the meso-RVE is characterized by its length L, width W, and height H, as well as the gap size S_{warp} between adjacent warp yarns, and the gap size S_{weft} between adjacent weft yarns. The cross-section of the yarn is usually assumed as an ideal ellipse shape with a and b denoting its major and minor axis, respectively. The undulation of each yarn is determined by altering the position of the control points (red dots in Fig. 2). Once the geometric parameters of the RVE are obtained, the 3D geometry and finite element mesh of the RVE can be generated using the open-source software package TexGen [31], which will be used as input for analysis within the proposed plugin AMWC.

Indeed, TexGen provides three types of commonly used meshing options to generate RVE models for woven composites, namely, volume mesh, voxel mesh, and dry mesh, each with distinct characteristics and applications as shown in Fig. 3. The volume mesh option generates a tetrahedral mesh that fills the entire volume of the textile composite, i.e., it creates a mesh consisting of tetrahedral elements for both the yarns and matrix, as the nodes are shared at the interface between the yarns and matrix. This facilitates the modeling of the interaction between the yarns and the matrix and allows for an accurate representation of the composite geometry, however, in cases of complex weave patterns it can be challenging to generate a perfect periodic tetrahedral mesh. In such cases, the voxel mesh may be more suitable. The voxel mesh option involves representing the RVE geometry using a grid of voxels, where each voxel corresponds to a cuboid or rectangular brick element. The advantage of this option is that it always generates periodic meshes for the RVE, but the tradeoff is that it requires a large number of elements to accurately represent complex weave patterns which can be computationally intensive. The third meshing option is dry mesh. This option creates a mesh of the yarns with cuboid or rectangular brick elements by excluding the matrix materials. The interaction between yarns within the dry mesh is modeled using cohesive contact behavior in the finite element method.

The finite element mesh of the RVE models will be exported to ABAQUS for calculation. Depending on the chosen mesh types and

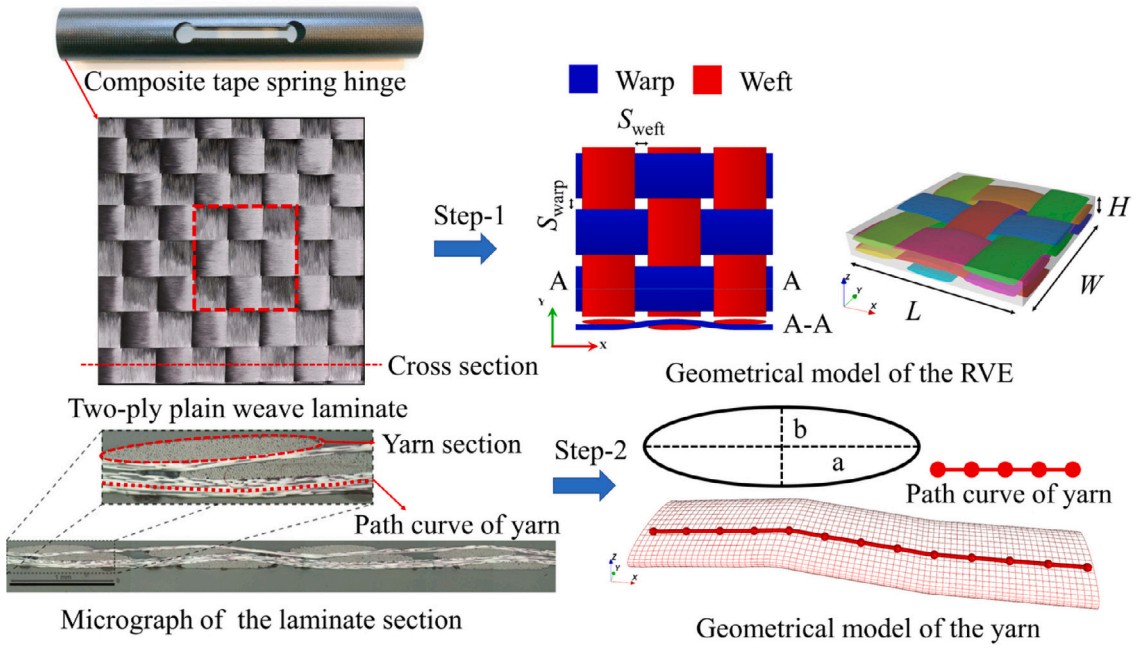

Fig. 2. Construction of a mesoscale RVE for woven composites. The weave pattern of the woven composite, the cross-sectional shape of the yarn, and the undulation path of the yarn are determined with precision through the use of an optical micrograph. The images of the composite tape-spring hinge and the micrograph of the woven composite are taken from Refs. [18,32], respectively.

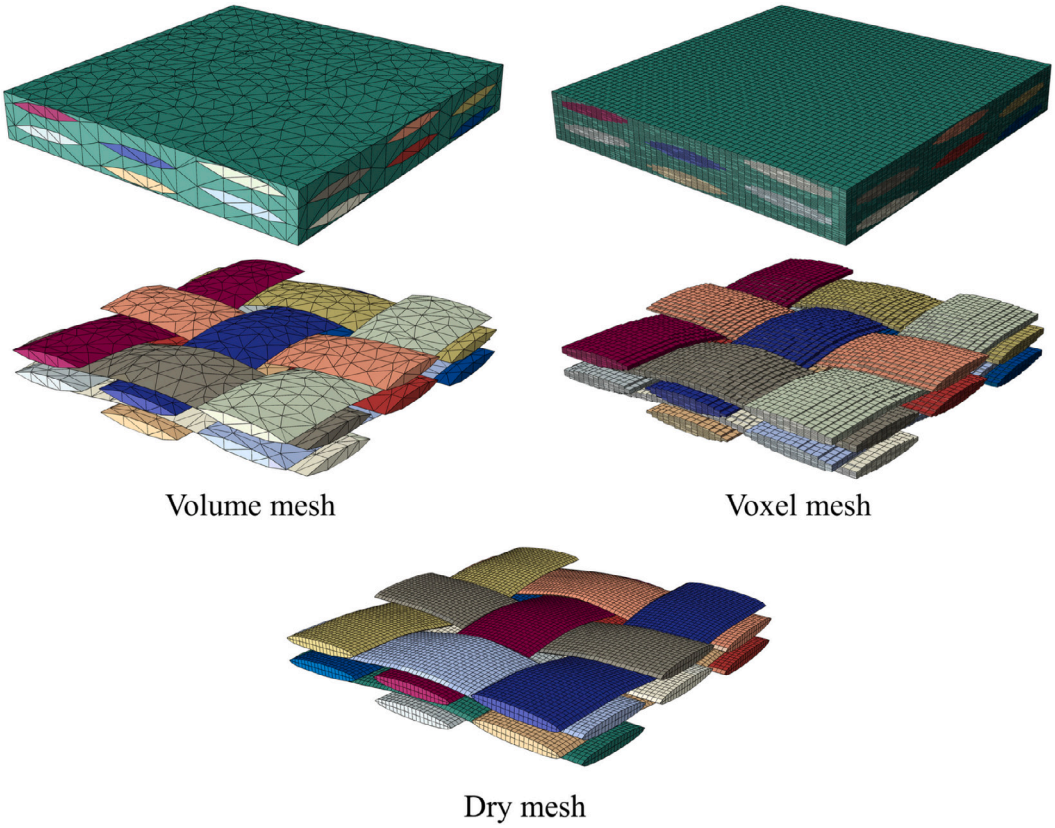

Fig. 3. Three commonly used meshing types for mesoscale RVE of woven composites in TexGen. Volume mesh generates a tetrahedral mesh of both the yarns and matrix. Voxel mesh generates a hexagonal mesh of both the yarns and matrix. Dry mesh generates a hexagonal mesh of only yarns.

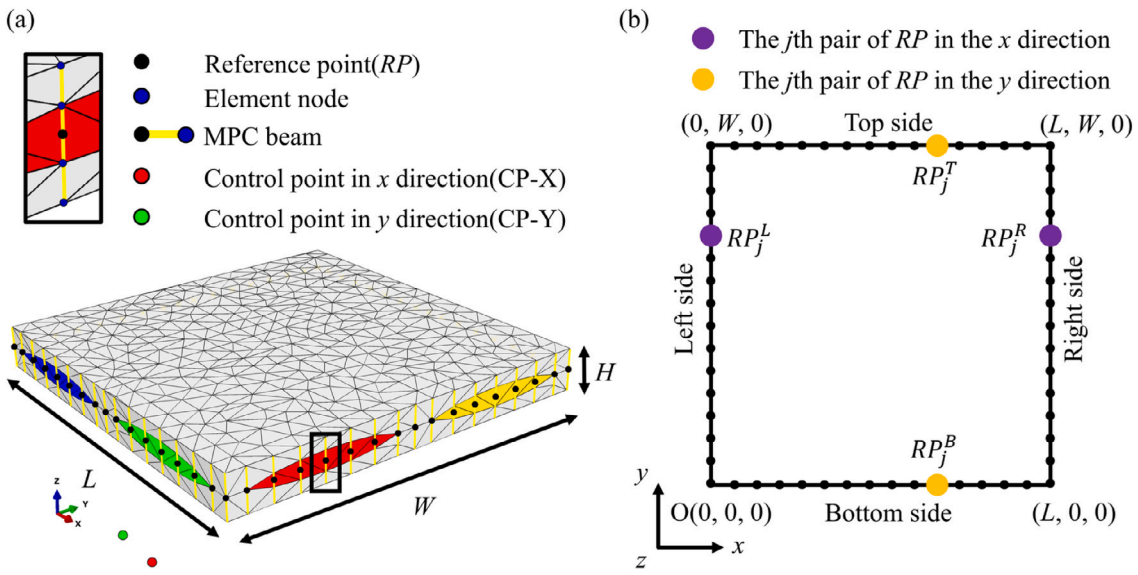

Fig. 4. Illustration of the finite element mesh of (a) RVE with MPC constraints on the side faces and (b) mid-plane schematic of a woven composite laminate.

material behaviors, different solution methods may be required when using ABAQUS. For the volume mesh and voxel mesh, which represent the matrix and yarns with shared nodes at the interface, the linear solution method (*Static, General in ABAQUS) is appropriate. This method assumes linear-elastic material behavior and is suitable for problems with small deformations and linear responses. On the other hand, for the dry fiber mesh, where the nodes at yarn interfaces are not shared, the general contact interaction function in ABAQUS is employed to model the interaction between yarns. This method involves automatic detection of contact pairs by ABAQUS contact algorithms, with the adoption of cohesive behavior as a contact property to simulate the separation and adhesion between adjacent yarns. Specifically, in the definition of cohesive behavior, stiffness values are assigned between the nodes in contact on the yarn surfaces to establish their association. The determination of these stiffness values requires the adoption of a cohesive traction-separation law, which defines the stress–displacement relationship between the adhesive surfaces, as shown in Eq. (2).

$$\begin{pmatrix} t_n \\ t_s \\ t_t \end{pmatrix} = \begin{bmatrix} k_{nn} & 0 & 0 \\ 0 & k_{ss} & 0 \\ 0 & 0 & k_{tt} \end{bmatrix} \begin{pmatrix} \delta_n \\ \delta_s \\ \delta_t \end{pmatrix} \tag{2}$$

where t and δ represent stress and separation displacement, respectively. The subscript n denotes the normal direction, while subscript s and subscript t represent the two transverse shear directions. The parameter k_{nn} corresponds to the normal stiffness, while k_{ss} and k_{tt} correspond to the shear stiffness in the two directions. Collectively, these parameters are referred to as the uncoupled traction stiffness [33], which characterizes the relationship between stress and separation displacement in the cohesive interface. The default contact enforcement method was taken in the simulations. It is important to note that the cohesive contact behavior may lead to convergence issues with the linear static analysis method. In such cases, the dynamic explicit solver (*Explicit, Dynamic in ABAQUS) is often preferred, which is well-suited for problems involving discontinuities. Before proceeding with the analysis, it is essential to assign the material properties of the yarns and matrix to their respective element sets in the mesh. In the meantime, implementing periodic boundary conditions and applying appropriate loading conditions allow us to investigate the response of the RVE under specific loads. These aspects will be elaborated on in the subsequent sections.

2.2. Implementation of periodic boundary conditions

Periodic boundary conditions are required to ensure the homogenization of the properties of the yarns and matrix in the mesostructure. For this study, we adopt the homogenized Kirchhoff plate theory proposed by Kueh and Pellegrino [17], which has been proven effective in accurately predicting the ABD matrix for woven composites [18,34]. As illustrated in Fig. 4, the elemental nodes lying on the lateral surfaces of the RVE are linked by means of rigid vertical beams (*MPC beam) to reference points lying in the mid-plane, and each reference point is related to the corresponding reference point at the opposite face by means of a constraint equation that enforces periodic boundary conditions. The equations that prescribe the relative displacements and rotations of the opposing reference points are given as follows:

$$u^{RP_j^R} - u^{RP_l^L} = \varepsilon_x L \tag{3}$$

$$u^{RP_j^T} - u^{RP_j^B} = \frac{1}{2}\gamma_{xy} W \tag{4}$$

$$v^{RP_j^R} - v^{RP_j^L} = \frac{1}{2}\gamma_{xy} L \tag{5}$$

$$v^{RP_j^T} - v^{RP_j^B} = \varepsilon_y W \tag{6}$$

$$\theta_x^{RP_j^R} - \theta_x^{RP_j^L} = -\frac{1}{2}\kappa_{xy} L \tag{7}$$

$$\theta_x^{RP_j^T} - \theta_x^{RP_j^B} = -\kappa_y W \tag{8}$$

$$\theta_y^{RP_j^R} - \theta_y^{RP_j^L} = \kappa_x L \tag{9}$$

$$\theta_y^{RP_j^T} - \theta_y^{RP_j^B} = \frac{1}{2}\kappa_{xy} W \tag{10}$$

$$w^{RP_j^R} - w^{RP_j^L} = -\frac{1}{2}\kappa_{xy} L y \tag{11}$$

$$w^{RP_j^T} - w^{RP_j^B} = -\frac{1}{2}\kappa_{xy} W x \tag{12}$$

where u, v, and w denote the translational displacements of the reference point in the x-, y-, and z-direction, and θ_x and θ_y denote the rotational displacements along the x- and y-direction, respectively. Superscripts RP_j^L, RP_j^R, RP_j^T, and RP_j^B represent the jth pair of reference points on the left, right, top, and bottom side of the RVE, as indicated by purple dots in Fig. 4(b). In practice, the degrees of freedom for each pair of reference points are linked to the corresponding degrees of freedom of a virtual node. Reference point pairs on the left and right lateral surfaces are related to the virtual node CP-X, while those on the top and

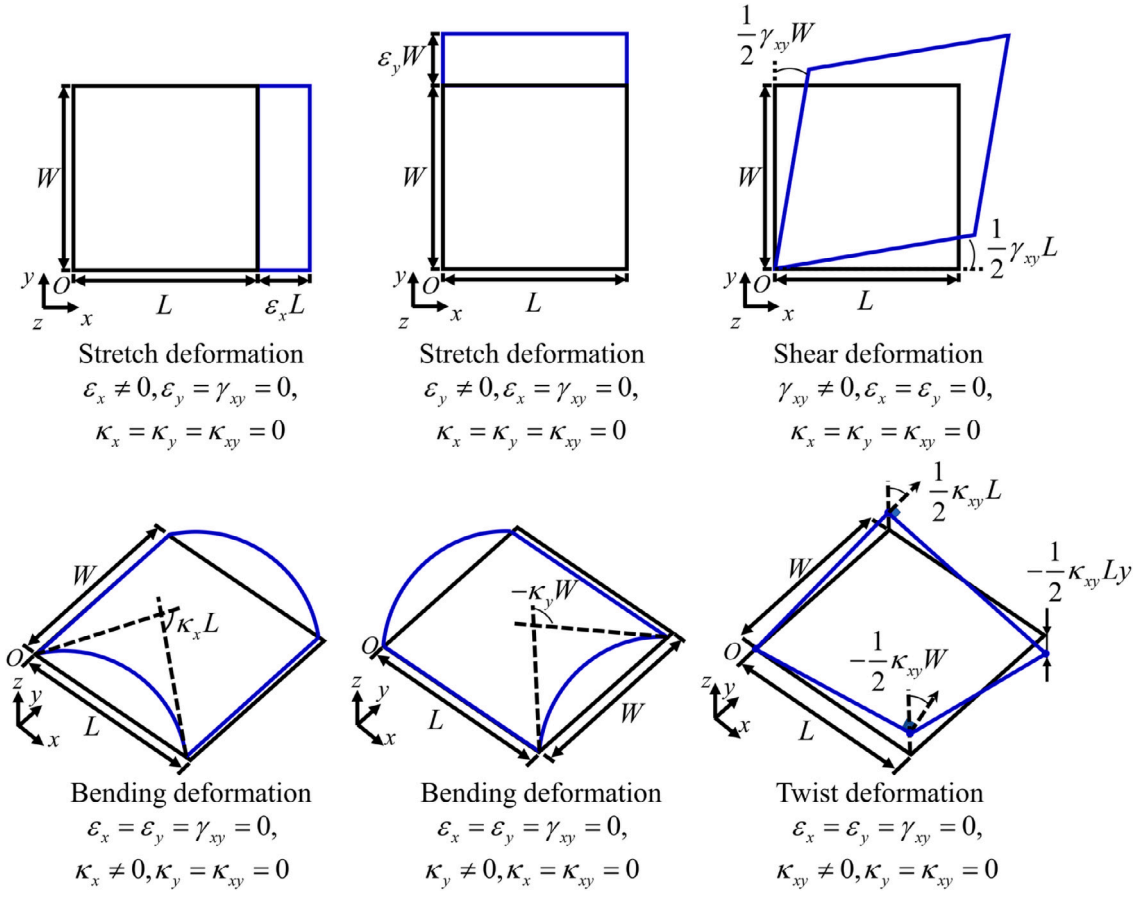

Fig. 5. Six specific cases of deformation for calculating all entries of the ABD matrix.

bottom surfaces are connected to the virtual node CP-Y. The specified displacements or rotations are assigned to the two virtual nodes, and the resulting forces or moments on the virtual nodes are computed as the resultant forces or moments exerted on the surface.

2.3. ABD matrix calculation

Finally, the entries in the ABD matrix can be determined by solving six specific loading cases, where for each case a constant strain vector is applied to the homogenized RVE, and the resulting reaction forces and moments are calculated. This process is illustrated in Fig. 5. For instance, in loading case 1, which involves the tension deformation in x-direction, a constant tensile strain ε_x is applied while all other strains are set to zero. By substituting $\varepsilon_x \neq 0$, $\varepsilon_y = \varepsilon_{xy} = \kappa_x = \kappa_y = \kappa_{xy} = 0$ into the Eq. (1), we can derive the first column entries of the ABD matrix as follows:

$$A_{11} = \frac{N_x}{\varepsilon_x}, A_{12} = \frac{N_y}{\varepsilon_x}, A_{16} = \frac{N_{xy}}{\varepsilon_x}, B_{11} = \frac{M_x}{\varepsilon_x}, B_{12} = \frac{M_y}{\varepsilon_x}, B_{16} = \frac{M_{xy}}{\varepsilon_x} \tag{13}$$

where $\varepsilon_x = u^{\mathrm{CP-X}}/L$ is the prescribed strain, and $N_x = F_x^{CP-X}/W, N_y = F_y^{CP-Y}/L, N_{xy} = F_y^{CP-X}/W, M_x = M_x^{CP-X}/W, M_y = M_y^{CP-Y}/L, M_{xy} = M_y^{CP-X}/W$ are the computed reaction forces/moments exerted on the virtual nodes. The remaining entries in the ABD matrix can be determined column by column by considering the other loading cases as depicted in Fig. 5.

3. AMWC software implementation

This section presents the implementation details of the ABAQUS plug-in AMWC. The aim of the plugin is to automate the process of homogenization as described above, thus enabling accurate prediction of the ABD matrix for woven composites. The plugin is implemented using the Python programming language and can be easily installed by placing the code package in the *abaqus_plugins* directory before launching the software. Once installed successfully, the AMWC option appears in the Plug-ins tab of the main menu bar in ABAQUS/CAE.

The GUI window of the AMWC plugin is illustrated in Fig. 6. To start with, users are required to import the finite element mesh of the meso-RVE from TexGen. Note that the imported mesh comes with some default settings, including material parameters for the yarns and the matrix, solver settings, constraint equations, boundary conditions, etc, which all should be removed before using AMWC for calculation. Thereafter, users are expected to provide the following parameters for model specification. First of all, the mesh type of the meso-RVE and the solver to be used for the analysis should be selected. Subsequently, users are prompted to input the model name and part name for identification, which can conveniently be found in the model tree within ABAQUS. Afterwards, the user needs to specify the number of yarns in the x- and y-directions, as well as the number of layers. Fig. 7 illustrates the default numbering system for different types of woven composites. Please be aware that when dealing with 2D weave composites, all of these numbers can be directly counted from the model. In the case of 3D woven composites, the number of yarns in x- and y-directions can be counted, and the layer number should be set to 1. The finite elements within the RVE are automatically categorized into three separate sets: those representing the yarns in the x-direction, those representing the yarns in the y-direction, and those associated with the matrix. Since the yarns are treated as orthotropic materials, it is necessary to define the material orientation in the simulation. The "1 direction" for the longitudinal orientation will be aligned with the direction of the yarns

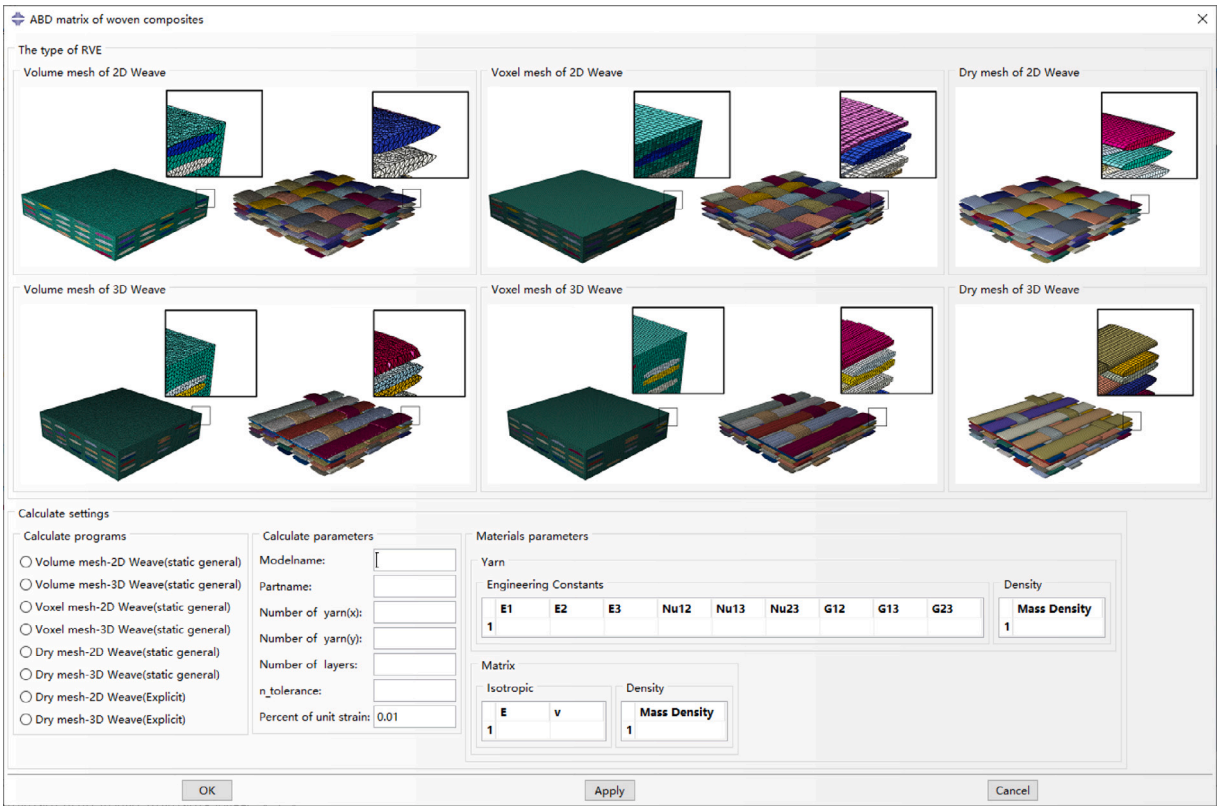

Fig. 6. GUI window of the *AMWC* plug-in.

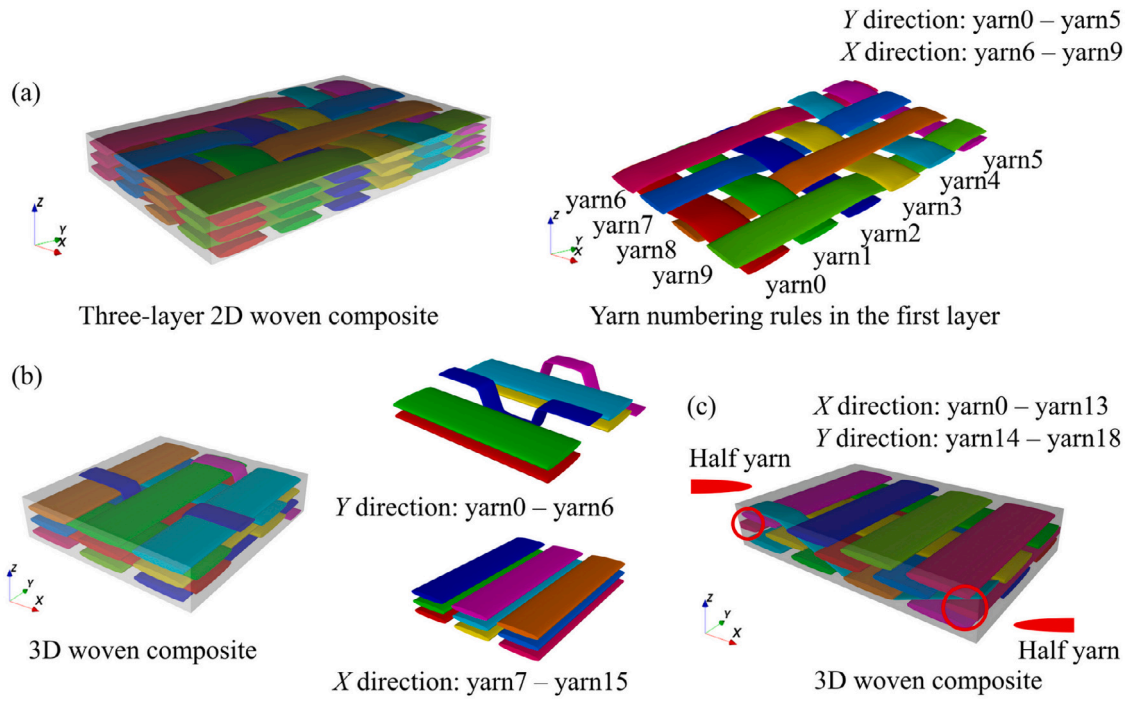

Fig. 7. Numbering scheme for different types of woven composite RVEs: (a) 2D Woven composite RVE; (b) 3D woven composite RVE; (c) 3D woven composite RVE with half-pick yarns. Two of the half-picks at the lateral surface are considered as one when counting the number of yarns.

in their respective sets. On the other hand, the matrix is treated as isotropic and does not require the specification of material orientation. The material properties for the yarns and the matrix should be input within the plugin interface. The density of the materials is also required for the use of the Explicit solver.

Furthermore, tolerance is a key parameter that controls the implementation of periodic boundary conditions. As has been described in Section 2, all nodes on lateral surfaces are extracted for the purpose of implementing periodic boundary conditions. However, in practice, elemental nodes may slightly deviate from the designated plane due to

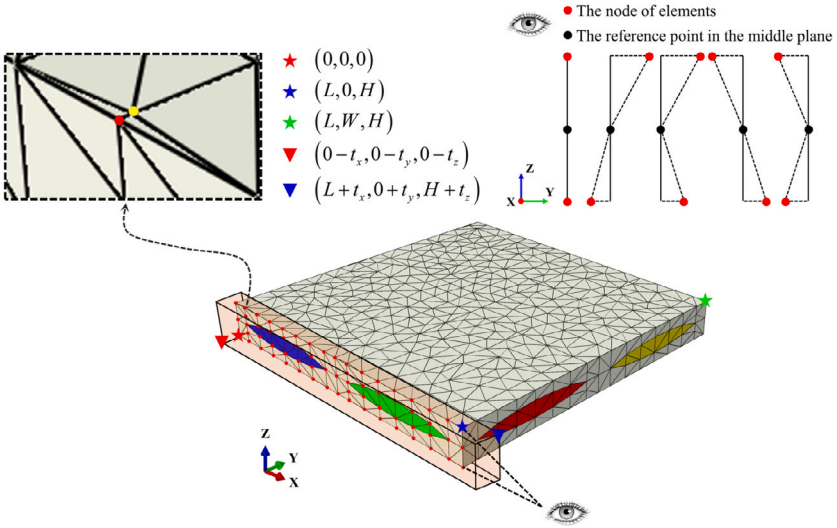

Fig. 8. Method for selecting nodes slightly deviated from the side surface of the RVE.

meshing errors, which can result in challenges when generating node sets. The tolerance is defined by dividing the total length L, width W, and height H of the RVE by a constant integer value denoted as n_{tol}. Consequently, the tolerance is used to make a cuboid region, and all nodes encompassed by the cuboid will be extracted to formulate the relevant constraint equations, see Fig. 8 for details. It is important to note that if the tolerance parameter n_{tol} is set to a large value, the tolerance is small and there might be issues with generating node sets due to mapping errors, which stops further operations. Conversely, if n_{tol} is set to a small value, there will be possibilities of linking more than two nodes in each constraint equation, potentially resulting in undesired over-constrained deformation. A default value of 250 is suggested for most cases for the parameter n_{tol}. However, its value can be adjusted based on the specific needs of each individual case. In situations only by adjusting the parameter n_{tol} does not yield satisfactory results, it might be necessary to create a more refined RVE mesh.

Finally, the analysis employs an applied strain of 0.01 as default. It should be clarified that in all simulations conducted using AMWC, a linear elastic deformation assumption is made. As a result, the magnitude of the applied strain does not change the calculation results of the ABD matrix. Therefore, a small value of the applied strain is recommended for saving computation costs. Once all of the above parameters are specified, AMWC will automate the implementation of periodic boundary conditions and the execution of the six specific simulations, as described in Section 2, as soon as the "Apply" button is clicked. After all the simulation jobs are done, AMWC automates a post-processing procedure, and the resulting ABD matrix for the analyzed meso-RVE will be saved in the ABAQUS work directory as a text file. The use of the plug-in with step-by-step procedures for calculating the ABD matrix of a 2D plain weave composite is presented as an example in Video S1 in the Supporting Information.

4. Numerical examples

In this section, a series of numerical examples are solved by AMWC and the results are compared with existing literature results to demonstrate the accuracy of AMWC. These examples include 2D weave composites, 3D woven composites, and multiaxial woven composites.

4.1. Plain weave composite

The first example features a double-layer plain weave composite studied by Mallikarachchi [18]. We start by creating the meso-RVE based on the geometric parameters as summarized in Table 1. It can be seen that a minor inconsistency exists between the geometry of the meso-RVE generated by TexGen and the model described in the literature [18]. This difference arises from the limitations of TexGen which prevent setting the gap size between adjacent yarns S to zero. Fig. 9 illustrates the RVE models generated in this study. All three types of meshing are used for the ABD matrix calculation in this case to make a comparison. The weave path of the yarn is defined by the coordinates of a set of control points as shown in Fig. 9b. Table 2 presents the material properties of the yarn and the matrix.

Table 3 presents a comparison between the results obtained using AMWC and the results reported in the literature [18], with the matrix entries equal to zero not shown. It can be seen that all three meshing types provide acceptable accuracy in predictions. Among these methods, the volume and voxel meshing methods demonstrate superior performance, showcasing more accurate results. Conversely, the dry mesh approach exhibits the most significant deviations, particularly in the tensile stiffness terms, which are mainly due to the setting of the adhesive contact properties (as defined in Eq. (2)). The tangential stiffness (k_{nn}, k_{ss} and k_{tt}) in the adhesive contact properties is typically determined through experimental testing [33], while in this study, the default settings in ABAQUS were temporarily adopted. Fig. 10(b) illustrates the strain distribution contour plots of the RVE (volume mesh model) under six different boundary conditions.

Subsequently, we conducted a verification of the AWMC for calculating the ABD matrix of [±45] double-layer plain weave composite materials. The material properties and internal geometric characteristics of this composite material match those of the previously discussed [0/90] double-layer plain weave composite precisely. In accordance with the periodic arrangement of [±45] ply orientations, there exist two distinct forms of RVE models, depicted in Fig. 11(a) and (b). It is important to note that the RVE model for the [±45] lay-up is more complex. Modeling employed Voxel mesh. The element size is set at 0.01980 × 0395980 × 002197, comprising a total of 500000 elements. In Fig. 11, the resin part is omitted for clarity. Given the striking similarity in the computational results of Model 1 and Model 2, Table 4 primarily displays the relative error between Model 2 and the results from Ref. [18]. Considering the consistent use of homogenization techniques, the minor discrepancies primarily originate from the differences in RVE geometric dimensions as shown in Table 1.

4.2. Satin weave composite

The following example features a single-layer satin weave composite studied by Sankar and Marrey [35]. The geometry configuration

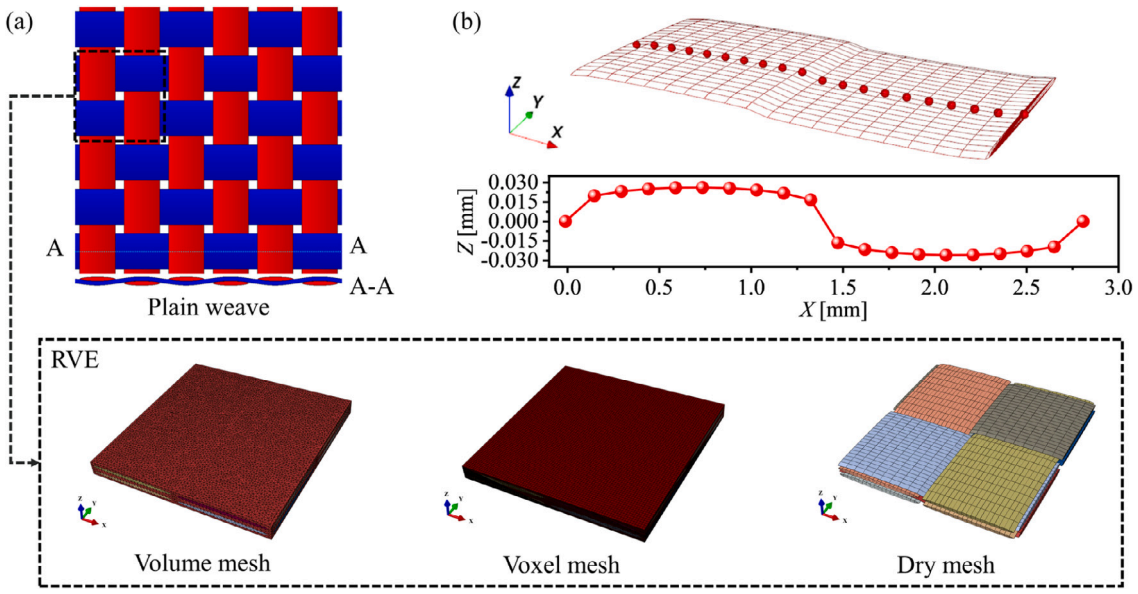

Fig. 9. Illustration of the RVE model for a double-layer plain weave composite.

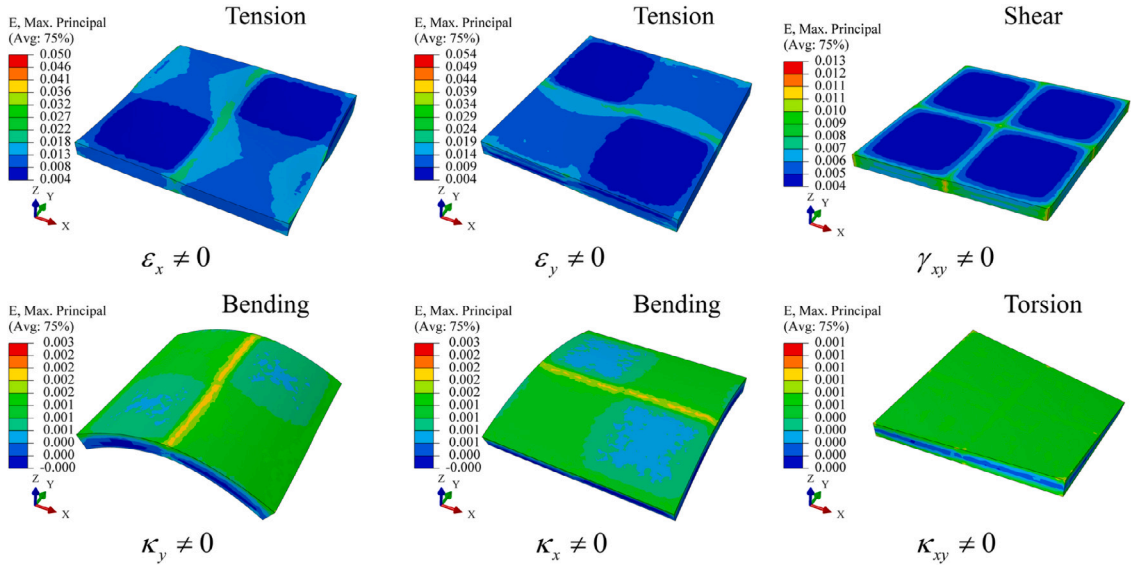

Fig. 10. Deformation of the meso-RVE with strain distribution for the six specific loading cases (Volume mesh).

Table 1
Geometric parameters for the meso-RVE of a double-layer plain weave composite.

RVE	L [mm]	W [mm]	H [mm]	S [mm]	a [mm]	b [mm]	Section area [mm^2]
This paper	2.8	2.8	0.219	0.068	0.666	0.0263	0.0589
Literature[18]	2.664	2.664	0.209	0	0.666	0.0262	0.0585

Table 2
Material properties for yarn and matrix.

Part	E_1 [MPa]	E_2 [MPa]	υ_{12}	υ_{23}	G_{12} [MPa]	G_{23} [MPa]
Yarn	159 520	11 660	0.267	0.472	3813	3961
Matrix	3390	3390	0.41	0.41	1210	1210

for the meso-RVE is shown in Fig. 12, and the associated geometric parameters are summarized in Table 5. The material properties of the yarn and matrix are outlined in Table 6. In this case, only the volume meshing method was employed for the calculation. The results presented in Table 7 mostly show good consistency, although notable relative errors are observed in the D matrix's bending stiffness terms. Similar to example 4.1, the computational errors primarily originate from differences in the RVE geometric models. However, the further

Table 3
ABD Matrix for Double-Layer Plain Weave Composite: AWMC Calculations vs. Literature [18].

Model	A_{11} [N/mm]	A_{12} [N/mm]	A_{22} [N/mm]	A_{66} [N/mm]
Volume mesh RVE	13 244.45	1024.03	13 246.9	684.21
Voxel mesh RVE	12 548.36	1095.64	12 548.36	677.61
Dry mesh RVE	12 098.77	1374.97	12 492.62	595.91
RVE[18]	13 009	1085	13 009	667
Experiment[18]	12 833 ± 517	–	–	785
Model	D_{11} [Nmm]	D_{12} [Nmm]	D_{22} [Nmm]	D_{66} [Nmm]
Volume mesh RVE	47.3	2.2	47.3	2.19
Voxel mesh RVE	41.05	1.93	41.05	1.94
Dry mesh RVE	40.09	1.47	40.98	1.56
RVE[18]	41.3	1.5	41.3	2.3
Experiment[18]	37.55 ± 5.54	–	–	–

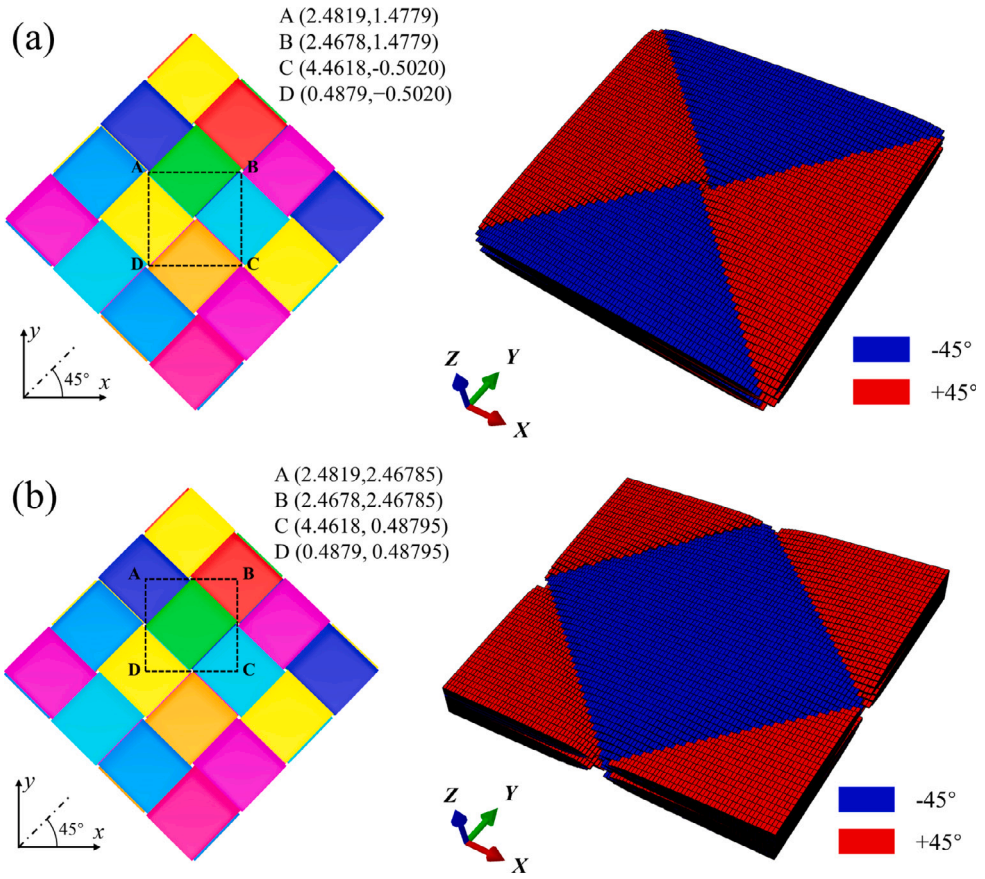

Fig. 11. RVE modeling schematic of [±45] double-layer plain weave composite material: (a) Model 1 and (b) Model 2.

Table 4
ABD Matrix for [±45] double-Layer plain weave composite: AWMC Calculations vs. Literature [18].

Model	A_{11} [N/mm]	A_{12} [N/mm]	A_{22} [N/mm]	A_{66} [N/mm]
Model 1	7360.30	5998.55	7344.41	5516.71
Model 2	7360.63	5998.40	7344.17	5515.49
Literature [18]	7714	6380	7714	5962
Error	4.58%	5.98%	4.79%	7.48%
Model	D_{11} [Nmm]	D_{12} [Nmm]	D_{22} [Nmm]	D_{66} [Nmm]
Model 1	23.40	18.32	23.37	19.06
Model 2	23.41	18.33	23.37	19.00
Literature [18]	23.6	19.1	23.6	19.9
Error	0.81%	4.03%	0.97%	4.52%

amplification of these errors can be attributed to the combined effect of two factors: the variance in yarn cross-sectional shape modeling between the Texcad software used by Sanker [35] and the Texgen software employed in our study, and the dimensional differences displayed in Table 5.

4.3. 3D woven composite

The subsequent example highlights a 3D woven composite model investigated by Liu et al. [30]. In this case, the accuracy of the ABD matrix prediction is verified by simulating the response of a shell

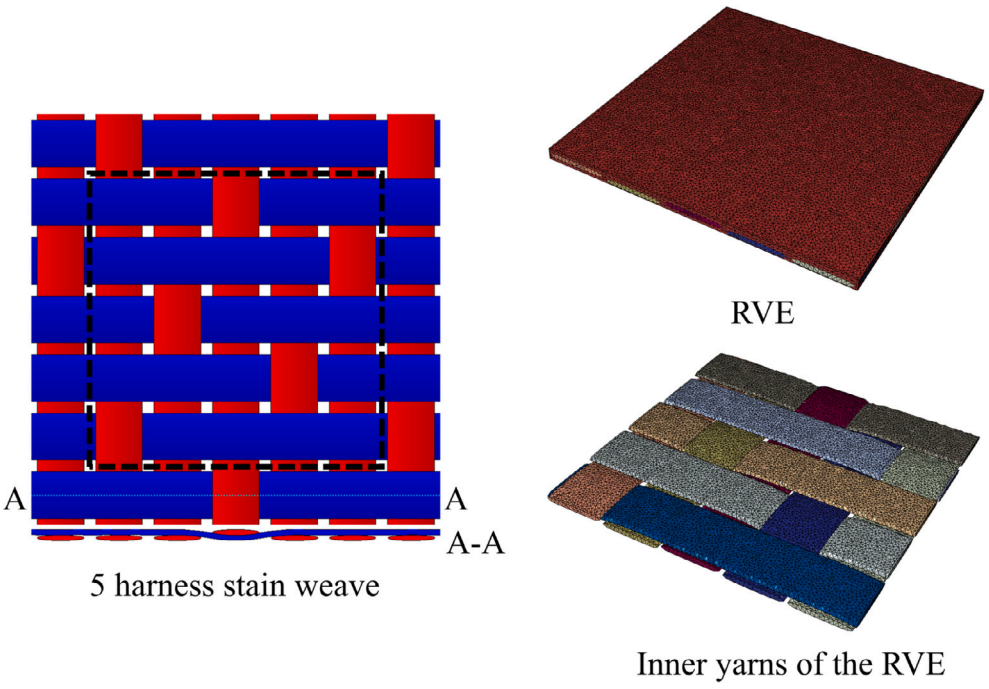

Fig. 12. Single layer 5-harness satin weave composite and RVE.

Table 5
Geometric parameters for the meso-RVE of a single-layer 5-harness satin weave composite.

RVE	L [mm]	W [mm]	H [mm]	S [mm]	a [mm]	b [mm]	Section area [mm^2]
This paper	7.5	7.5	0.2813	0.0445	0.157	0.705	0.0639
Literature [35]	7.055	7.055	0.2557	0	0.15386	0.705	0.0639

Table 6
Material properties for the yarns and matrix.

Part	E_1 [MPa]	E_2 [MPa]	υ_{12}	υ_{23}	G_{12} [MPa]	G_{23} [MPa]
Yarn	144 800	11 730	0.230	0.300	5520	4512
Matrix	3450	3450	0.35	0.35	1210	1210

Table 7
ABD Matrix for Single-Layer Satin Weave Composite: AWMC Calculations vs. Literature [35].

Model	A_{11} [N/mm]	A_{12} [N/mm]	A_{22} [N/mm]	A_{66} [N/mm]
Volume mesh RVE	14 309.3	1287.27	14 274.0	1159.72
RVE [35]	14 683	1351	14 683	1210
Error	2.55%	4.72%	2.79%	4.16%
Model	B_{11} [N]	B_{12} [N]	B_{22} [N]	B_{66} [N]
Volume mesh RVE	463.36	0	−461.76	0
RVE [35]	495	0	−495	0
Error	6.39%	0.00%	6.72%	0.00%
Model	D_{11} [Nmm]	D_{12} [Nmm]	D_{22} [Nmm]	D_{66} [Nmm]
Volume mesh RVE	78.96	2.15	78.37	6.16
RVE [35]	90.07	1.123	90.07	6.15
Error	12.33%	47.77%	12.98%	0.162%

structure and comparing the results with those obtained from a high-resolution 3D model. The workflow for this analysis is depicted in Fig. 13. To simulate the response of a plate composed of 3D woven composites, two methods are typically employed. One method involves directly discretizing the finite-sized structure with a huge number of solid elements to generate a high-resolution 3D finite-element model, which is referred to as the direct numerical simulation (DNS) method. The other approach involves first homogenizing the properties of the composites through meso-RVE analysis and then utilizing the ABD matrix to simulate the response of the homogenized structure. The DNS results serve as a benchmark for evaluating the accuracy of the ABD matrix calculation. The model considered here is taken from the literature [30], where the ABD matrix of a 3D woven composite was calculated using a structural genome method, and a high-resolution 3D model for the finite-sized structure was also established and solved for validation purposes. As depicted in Fig. 13, the overall dimensions of the finite-sized structure are 85.71 mm × 102.85 mm × 2.00 mm. A mesoscale RVE is selected within this overall model based on periodicity. The RVE has a spacing of 4.286 mm between warp and weft yarns, a width of 3.428 mm, and a height of 0.286 mm. The bound yarn had a width of 1.714 mm and a height of 0.286 mm. The material properties of the yarns and the matrix are described in Table 8. The ABD matrix

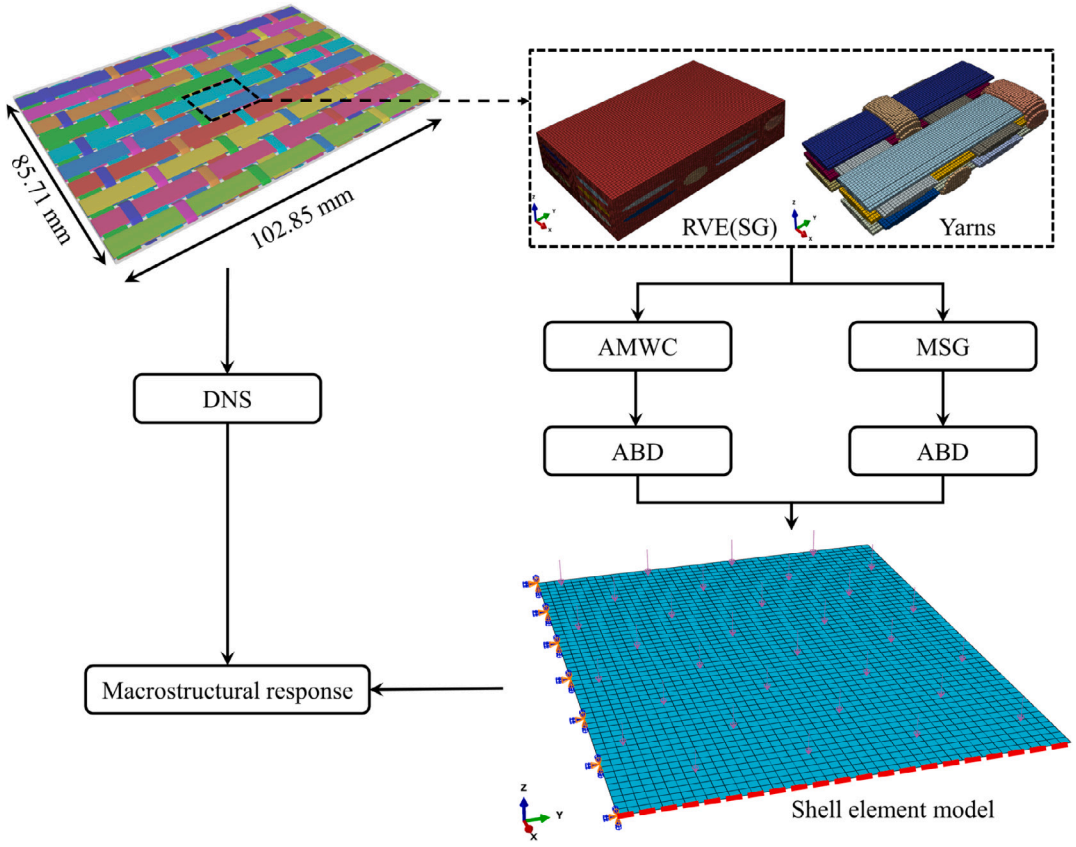

Fig. 13. Multiscale analysis workflow for 3D orthogonal woven composite plate structure.

Table 8
Material properties for the yarns and matrix for a 3D woven composite.

Part	E_1 [MPa]	E_2 [MPa]	υ_{12}	υ_{23}	G_{12} [MPa]	G_{23} [MPa]
Yarn	126 910	16 490	0.260	0.440	3720	3220
Matrix	4510	4510	0.38	0.38	1700	1700

predictions obtained using the AMWC method were compared with the results predicted by MSG presented in literature [30], as shown in Table 9. The table reveals that the ABD matrices calculated by both methods are generally in good agreement, with the notable exception of a significant discrepancy in the A_{12} component. Since both SG and RVE employed identical finite element models (including geometric parameters and mesh), this error is likely attributable to differences between the RVE and MSG homogenization theories. Subsequently, the ABD matrix is utilized to simulate the macroscopic response of the finite-sized structure. One edge of the model was fully fixed, while the other three edges were left free. A uniform pressure of 0.01 MPa was applied to the upper surface in a downward direction. The nodal displacements in z-direction along the plate edge red dashed line in Fig. 13 were extracted to facilitate a comparison. The results obtained from the high-resolution 3D model, computed using the ABD matrix predicted by AWMC and the structural genome method are all presented in Fig. 14, demonstrating a high level of consistency across the three sets of results.

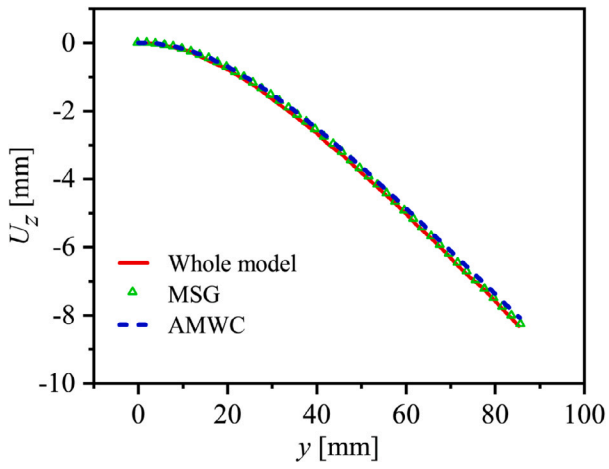

Fig. 14. Z-direction nodal displacements predicted by three methods.

4.4. Triaxial weave composite

This example showcases a single-layer triaxial weave composite as studied by Kueh and Pellegrino [17]. As depicted in Fig. 15(a), the triaxial weave employs yarns woven together at three different angles, resulting in a distinctive fabric construction. The meso-RVE geometry for this triaxial weave composite is defined by the parameters summarized in Table 10. Kueh and Pellegrino employed beam elements to approximate the yarns and constructed an RVE finite element model as depicted in Fig. 16(b). While this approach significantly improves computational efficiency, it may lead to the loss of some structural features in the RVE. In this work, a 3D finite element model of the meso-RVE is constructed, as depicted in Fig. 15(c). Furthermore, Table 11 provides

Table 9
Comparison of ABD matrix calculation results.

Model	A_{11} [N/mm]	A_{12} [N/mm]	A_{22} [N/mm]	A_{66} [N/mm]
Voxel mesh RVE	47 536.5	6258.4	85 643.8	4938.9
MSG [30]	45 902.4	5581.3	80 702.0	4844.8
Error	3.55%	12.13%	6.12%	1.94%
Model	D_{11} [Nmm]	D_{12} [Nmm]	D_{22} [Nmm]	D_{66} [Nmm]
Volex mesh RVE	8319.6	1733.6	18 694.5	1413.1
MSG [30]	8144.7	1618.4	18 855.0	1429.5
Error	2.14%	7.12%	0.85%	1.15%

Table 10
Geometric parameters of meso-RVE for the triaxial weave composite.

Parameters	Δl_x	Δl_y	Δl_z	a	b_i	b_{ii}	b_{iii}	c	d
Volume mesh RVE	3.12	5.4	0.039	2.7378	4.0524	2.0262	0.6754	0.803	0.078

Table 11
Material properties for the yarns in the triaxial weave composite.

Part	E_1 [MPa]	E_2 [MPa]	υ_{12}	υ_{23}	G_{12} [MPa]	G_{23} [MPa]
Yarn	157 650	13 280	0.256	0.300	4561	1745

Table 12
Comparison of ABD matrix calculation results.

Model	A_{11} [N/mm]	A_{12} [N/mm]	A_{22} [N/mm]	A_{66} [N/mm]
Volume mesh RVE	3016.06	1684.76	3042.87	679.18
Beam element RVE [17]	3411.10	2050.20	3411.00	680.42
Error	11.58%	17.82%	10.79%	0.182%
Experiment [17]	3106.9 ± 76	1552.66	3106.9 ± 76	777.12 ± 74
Model	D_{11} [Nmm]	D_{12} [Nmm]	D_{22} [Nmm]	D_{66} [Nmm]
Volume mesh RVE	2.24	0.54	2.21	0.47
Beam element RVE [17]	2.17	0.64	2.17	0.78
Error	3.22%	15.62%	1.84%	39.74%
Experiment [17]	2.077 ± 0.05	–	2.077 ± 0.05	–

Table 13
Material properties for the yarn and matrix.

	Transversely isotropic yarn				Isotropic resin		
	E_{11} [MPa]	E_{22} [MPa]	G_{12} [MPa]	G_{23} [MPa]	υ_{12}	E [MPa]	υ
Plate	180 000	60 000	64 000	23 000	0.4	40 000	0.3
Shell	139 840	6400	3770	2360	0.22	3000	0.36

the material properties for the yarns within the triaxial weave composite. It is important to note that, owing to the intricate nature of yarn orientations within triaxial weave composites, the AMWC plug-in does not currently offer an interface for calculating the ABD matrix for such materials. Nevertheless, the analysis was conducted using the AMWC code programs. Table 12 presents the calculation results alongside a comparison with the results from the literature [17]. The results reveal significant relative errors in several stiffness components, with the beam model consistently yielding higher estimates. This discrepancy largely stems from Kueh's model treating yarn interactions as rigid Tie connections. Consequently, AMWC's predictions more closely resemble experimental data, surpassing Kueh's model. This improvement is credited to the three-dimensional RVE finite element mesh used in this study, offering a more precise representation of both the geometric and contact characteristics of the RVE. Furthermore, this case study demonstrates the AMWC program's capability to accurately predict the ABD matrix for a diverse range of woven composite materials.

4.5. Accuracy of shell element with ABD matrix

To validate the accuracy of the shell elements of the ABD matrix calculated using AMWC, this study selected two cases. The first case concerns a single-layer plain weave composite plate as depicted in Fig. 17(a), employing a 1/4 symmetric model. The plate has dimensions of 128 mm in both length and width, with a thickness of 3.8 mm. The yarns of the woven composite material have an elliptical cross-section, with a major axis of 6.0 mm and a minor axis of 1.5 mm, and their undulating path follows the pattern of $1.0\sin(\pi/8)$. Each Representative Volume Element (RVE) measures 16 mm in length and width, and 3.8 mm in thickness, with the entire plate comprising 16×16 RVEs. In the illustrated 1/4 symmetric model, one set of adjacent edges is fully fixed, while the other set is subjected to symmetric boundary conditions. The second case involves a single-layer plain weave composite curved shell as shown in Fig. 17(b). Detailed geometric parameters of both the curved shell and the yarns are provided in the figure. The RVE dimensions for the curved shell are identical to those of the plate, and the entire shell comprises 16 RVEs. One side of the curved shell is fully fixed, and a uniform pressure of 0.1 MPa is applied to the upper surface. Material parameters for the yarns and resin used in the woven composite materials of both the plate and curved shell are listed in Table 13.

Three distinct approaches were employed to model and compute the structures of the aforementioned plate and curved shell. The first method involved the use of C3D8 solid elements in ABAQUS to discretize the woven composite plate and curved shell structures as shown in Fig. 17, thereby establishing a high-precision finite element model for the direct solution of structural responses. The second approach, based on the embedded element method and the solid-shell concept

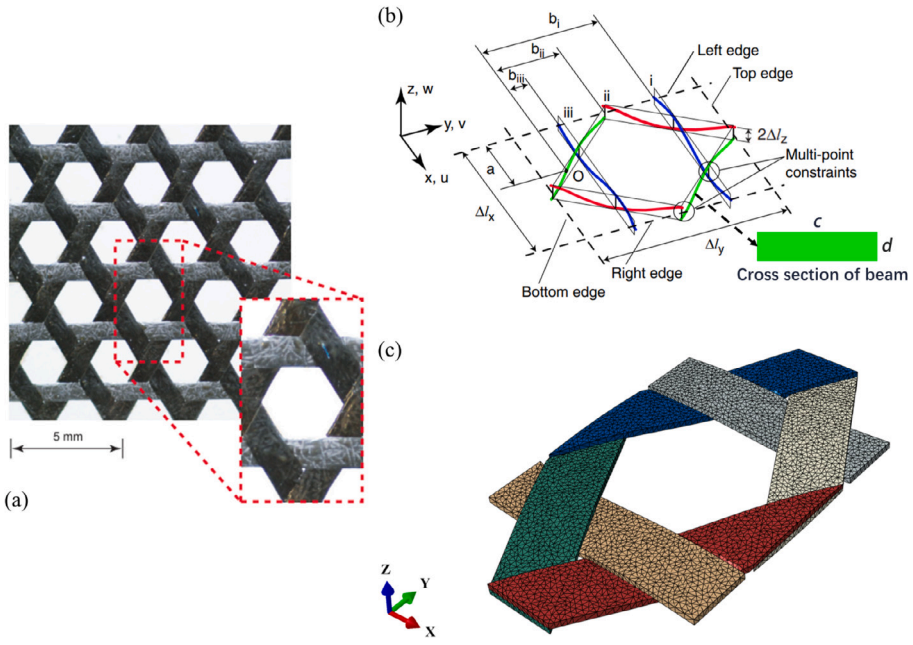

Fig. 15. Triaxial weave composite and its RVE: (a) Single-layer triaxial woven composite material; (b) RVE with a beam element finite element model; (c) RVE with a solid element finite element model.

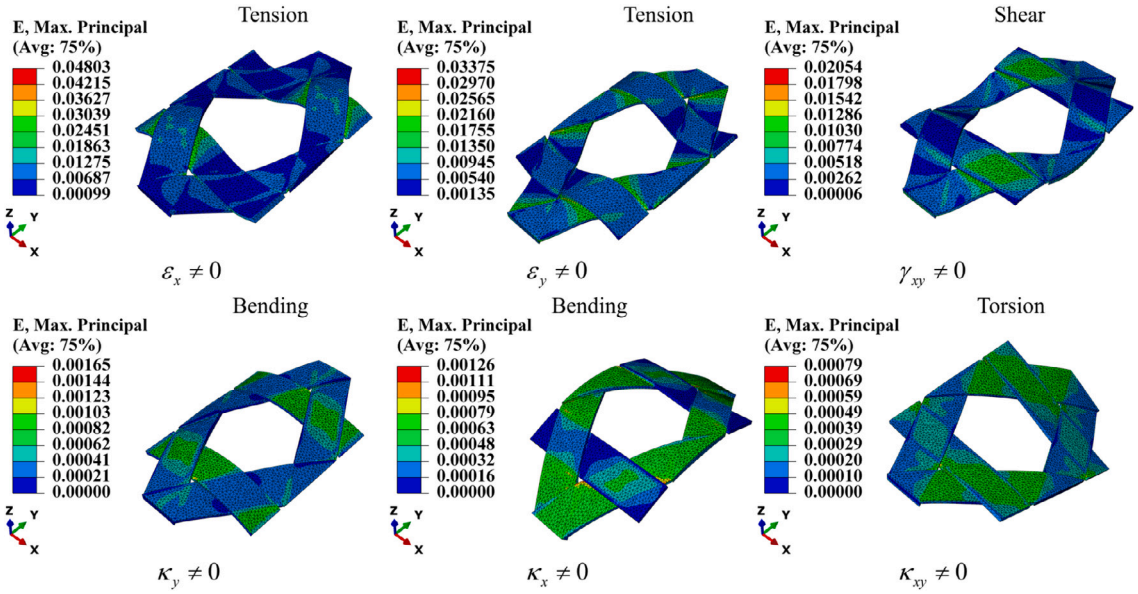

Fig. 16. Deformation of the meso-RVE for a triaxial weave composite with strain distribution for the six specific loading cases.

proposed by Xu and M. Waas, integrates the structural and material characteristics of the RVE into a single shell element [36]. This element, referred to hereafter as the S25 element, is suitable for the analysis of planar and curved structures. Utilizing this element, finite element models of the plate and curved shell were constructed, and the structural responses were resolved. Detailed descriptions of these two methods and the settings of the finite element models can be found in the relevant literature [36]. The third approach, which is the method of this paper, involves the creation of finite element models for the plate and curved shell RVEs as depicted in Fig. 17 using Texgen. The models utilized C3D10 elements with an average element size of 0.4 mm and total element counts of 160228 and 162221, respectively, and underwent mesh independence verification. The ABD matrices were calculated using AMWC, as presented in Table 14. In ABAQUS, the finite element models shown in Fig. 16 were constructed using S4 shell elements with an element size of 3.2 mm and a total count of 400, also undergoing mesh independence verification. The macroscopic responses of the structures were calculated using the Static, General solver (*Nlgeom = ON) with the ABD matrices input from Table 14.

Fig. 18 illustrates the results of finite element analyses for woven composite plate and curved shell structures using the three different types of elements mentioned: C3D10 solid elements, S25 shell elements, and S4 shell elements (AMWC). The deformation differences in the

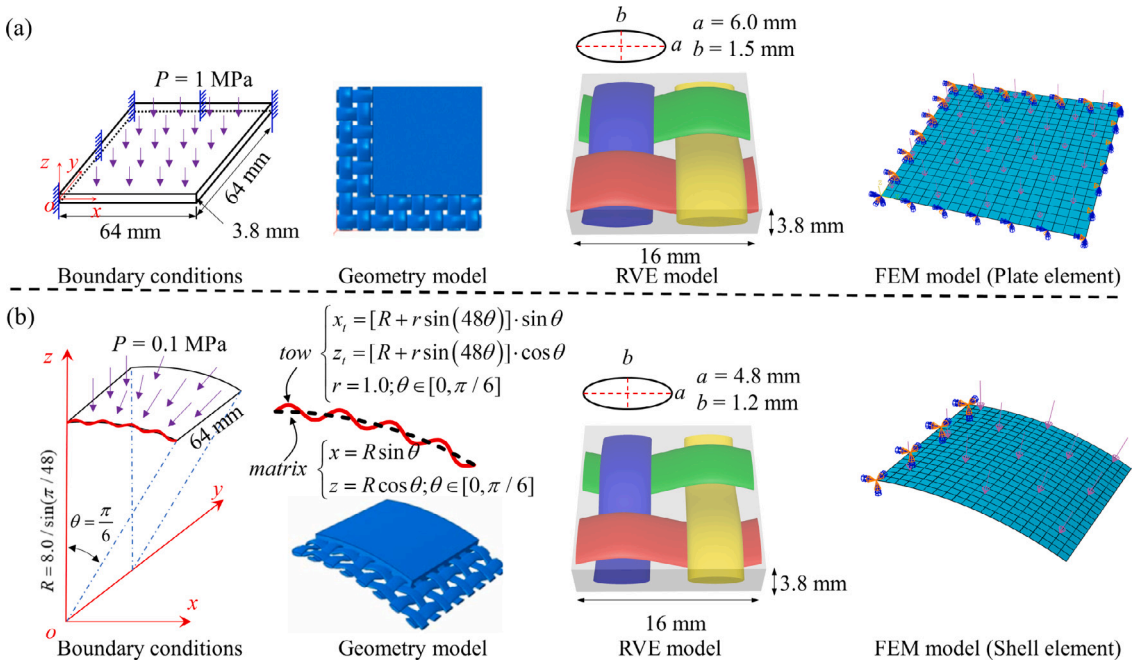

Fig. 17. Multiscale models of a single-layer plain weave composite material plate and shell structures. (a) Boundary conditions, geometric model, and the RVE-based homogenization model of a composite material plate (1/4 symmetric model). One set of adjacent edges is fully fixed, while the other set is subject to symmetric boundary conditions, with a uniform pressure of 1 MPa applied on the upper surface. (b) Boundary conditions and geometric model of a composite material curved shell, along with the RVE-based homogenization model: one edge of the shell is fully fixed, and a uniform pressure of 0.1 MPa is applied on the upper surface.

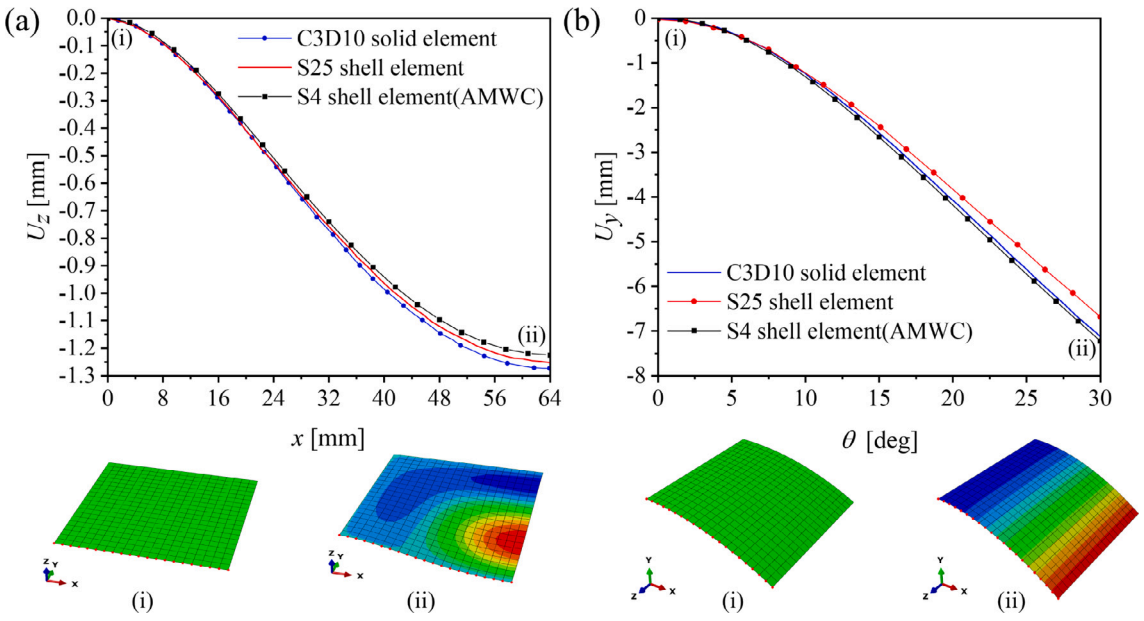

Fig. 18. Comparison of the deformation in the thickness direction along red edge between FEA used three types of element, C3D10, S25 and S4: (a) Woven composite plate; (b) Woven composite curved shell.

Table 14
ABD matrix for the woven plate and shell.

	A_{11} [N/mm]	A_{12} [N/mm]	A_{22} [N/mm]	A_{66} [N/mm]	D_{11} [Nmm]	D_{12}[Nmm]	D_{22}[Nmm]	D_{66}[Nmm]
Plate	294 640	77 460	294 640	120 070	272 570	68 820	272 570	91 720
Shell	42 790	8740	42 790	6280	26 460	6240	26 460	5680

thickness direction along the red-highlighted edges of the finite element models are compared. Fig. 18(a) depicts the variation of the thickness direction displacement U_z with respect to the x coordinate along the edge of the plate. From the graph, it can be observed that the predictions of C3D10 solid elements, S25 shell elements, and S4 shell elements (AMWC) are in good agreement. The maximum relative error of S4 shell elements (AMWC) with respect to the two reference results is 4.3%, occurring at $x = 64$ mm. Fig. 18(b) presents the variation of U_y along the θ coordinate along the edge of the curved shell. Similarly, the simulation results of the three types of elements nearly overlap, with S4 shell elements (AMWC) closely approaching the response of C3D10 solid elements, with a maximum error occurring at $\theta = 30$ degrees, which is only 1.13%.

5. Conclusion

Woven composites exhibit excellent mechanical properties owing to their rich micro-geometric features, making them highly valuable for wide applications in aerospace, automobile, and civil engineering. However, predicting the ABD matrix of woven composites is challenging due to the complex heterogeneity. The classical laminate theory has shown limitations in accurately predicting the ABD matrix for woven composites, particularly in cases where the calculation of bending stiffness is concerned. On the other hand, the numerical homogenization approach has been proven as an effective method to predict the ABD matrix for a wide range of woven composites. However, the process of constructing the mesoscale RVE, accurately implementing the necessary periodic boundary conditions, and applying the specific loading conditions remains intricate, which still hinders the widespread use of the method.

To address this issue, this paper develops an ABAQUS plugin tool named "ABD Matrix of Woven Composite (AMWC)" that simplifies the calculation procedures of the ABD matrix for woven composites. The mesoscale RVE of a woven composite could be generated using the open-source software TexGen. Afterwards, the finite element mesh of the RVE is imported into ABAQUS. AWMC then automates the setup of periodic boundary conditions, sequentially applies six predefined loading conditions, and calculates the ABD matrix for the laminate as the final output. All these features are achieved within a simple and user-friendly interface, eliminating the need for further programming and analysis by users, thereby saving time and effort and allowing users to focus more on the design of woven composites. The efficiency of the plugin tool was validated through a series of benchmark examples, including 2D woven composites, 3D woven composites, multiaxial woven composites, and curved shell structures of woven composites. In these case studies, the AMWC calculation results showed some degree of error relative to the benchmark data. These errors can be attributed to two main factors: (1) minor inaccuracies in the RVE geometric model; and (2) differences in the homogenization theories. Although these errors have been demonstrated to be negligible in the macroscopic response analysis of simple structures, a precise quantitative study on the impact of each stiffness component's error on the structural response is still needed. This will guide further improvements in the predictive accuracy of AMWC. By making the source code of the plugin tool publicly available to the community, we hope to provide an accessible and user-friendly homogenization approach for predicting the ABD matrix of a wide range of woven composites.

CRediT authorship contribution statement

Hao Jin: Data curation, Formal analysis, Investigation, Methodology, Software, Validation, Visualization, Writing – original draft, Writing – review & editing. **Ning An:** Writing – original draft, Writing – review & editing. **Qilong Jia:** Resources. **Xiaofei Ma:** Project administration, Resources. **Jinxiong Zhou:** Project administration, Resources, Supervision, Writing – review & editing.

Declaration of competing interest

The authors declare the following financial interests/personal relationships which may be considered as potential competing interests: Jinxiong Zhou reports financial support was provided by National Natural Science Foundation of China. Jinxiong Zhou reports financial support was provided by Fundamental Research Funds for the Central Universities. Ning An reports financial support was provided by State Key Laboratory of Structural Analysis for Industrial Equipment, Dalian University of Technology.

Data availability

The source codes of the plug-in tool as well as the benchmark input files are published open-source and can be downloaded from https://github.com/XJTU-Zhou-group/ABAQUS-Plugin-of-ABD-matrix.

Acknowledgments

This research is supported by the National Natural Science Foundation of China (grants 12202295 and 11972277), the Fundamental Research Funds for the Central Universities, China (grant YJ2021137), and the Open Project of State Key Laboratory of Structural Analysis for Industrial Equipment, Dalian University of Technology (No. GZ22120). The authors also thank Professor Chinthaka Mallikarachchi at the University of Moratuwa for helpful discussions.

References

[1] Li J, Lee JD, Chong KP. Multiscale analysis of composite material reinforced by randomly-dispersed particles. Int J Smart Nano Mater 2012;3(1):2–13.
[2] Ma X, Li T, Ma J, Wang Z, Shi C, Zheng S, et al. Recent advances in space-deployable structures in China. Engineering 2022;17:207–19.
[3] Kaw AK. Mechanics of composite materials. CRC Press; 2005.
[4] Zhang C, Binienda WK, Kohlman LW. Analytical model and numerical analysis of the elastic behavior of triaxial braided composites. J Aerosp Eng 2014;27(3):473–83.
[5] Dang H, Liu P, Zhang Y, Zhao Z, Tong L, Zhang C, et al. Theoretical prediction for effective properties and progressive failure of textile composites: A generalized multi-scale approach. Acta Mech Sin 2021;37:1222–44.
[6] Dang H, Zhao Z, Liu P, Zhang C, Tong L, Li Y. A new analytical method for progressive failure analysis of two-dimensional triaxially braided composites. Compos Sci Technol 2020;186:107936.
[7] Dang H, Zhang Y, Liu P, Zhao Z, Tong L, Zhang C, et al. Progressive failure prediction of three-dimensional woven composites using a generic multi-scale analytical model. Compos Struct 2023;303:116321.
[8] Hallal A, Younes R, Fardoun F. Review and comparative study of analytical modeling for the elastic properties of textile composites. Composites B 2013;50:22–31.
[9] Ishikawa T, Chou T-W. Elastic behavior of woven hybrid composites. J Compos Mater 1982;16(1):2–19.
[10] Ishikawa T, Chou TW. Stiffness and strength behaviour of woven fabric composites. J Mater Sci 1982;17:3211–20.
[11] Angioni SL, Meo M, Foreman A. A critical review of homogenization methods for 2D woven composites. J Reinf Plast Compos 2011;30(22):1895–906.

[12] Gommers B, Verpoest I, Van Houtte P. The Mori–Tanaka method applied to textile composite materials. Acta Mater 1998;46(6):2223–35.
[13] Verpoest I, Lomov SV. Virtual textile composites software WiseTex: Integration with micro-mechanical, permeability and structural analysis. Compos Sci Technol 2005;65(15–16):2563–74.
[14] Soykasap Ö. Micromechanical models for bending behavior of woven composites. J Spacecr Rockets 2006;43(5):1093–100.
[15] Sankar BV, Marrey RV. Analytical method for micromechanics of textile composites. Compos Sci Technol 1997;57(6):703–13.
[16] Naik RA. Analysis of woven and braided fabric-reinforced composites. ASTM Special Tech Publ 1996;1274:239–63.
[17] Kueh A, Pellegrino S. ABD matrix of single-ply triaxial weave fabric composites. In: 48th AIAA/aSME/ASCE/AHS/aSC structures, structural dynamics, and materials conference. 2007, p. 2161.
[18] Mallikarachchi H. Predicting mechanical properties of thin woven carbon fiber reinforced laminates. Thin-Walled Struct 2019;135:297–305.
[19] Gao J, Chen W, Yu B, Fan P, Zhao B, Hu J, et al. A multi-scale method for predicting ABD stiffness matrix of single-ply weave-reinforced composite. Compos Struct 2019;230:111478.
[20] Yu W. A unified theory for constitutive modeling of composites. J Mech Mater Struct 2016;11(4):379–411.
[21] Deo A, Yu W. Equivalent plate properties of composite corrugated structures using mechanics of structure genome. Int J Solids Struct 2021;208:262–71.
[22] Liu N, Yu W. Mechanics of structure genome-based buckling analysis of sandwich structures. Thin-Walled Struct 2021;169:108364.
[23] Liu X, Peng B, Yu W. Multiscale modeling of the effective thermal conductivity of 2D woven composites by mechanics of structure genome and neural networks. Int J Heat Mass Transfer 2021;179:121673.
[24] Tao F, Lyu X, Liu X, Yu W. Multiscale analysis of multilayer printed circuit board using mechanics of structure genome. Mech Adv Mater Struct 2021;28(8):774–83.
[25] Liu X, Rouf K, Peng B, Yu W. Two-step homogenization of textile composites using mechanics of structure genome. Compos Struct 2017;171:252–62.
[26] Kwok K, Pellegrino S. Micromechanics models for viscoelastic plain-weave composite tape springs. Aiaa J 2017;55(1):309–21.
[27] Ye F, Wang H. A simple python code for computing effective properties of 2D and 3D representative volume element under periodic boundary conditions. 2017, arXiv preprint arXiv:1703.03930.
[28] Omairey SL, Dunning PD, Sriramula S. Development of an ABAQUS plugin tool for periodic RVE homogenisation. Eng Comput 2019;35:567–77.
[29] An N, Jia Q, Jin H, Ma X, Zhou J. Multiscale modeling of viscoelastic behavior of unidirectional composite laminates and deployable structures. Mater Des 2022;219:110754.
[30] Liu X, Gasco F, Yu W, Goodsell J, Rouf K. Multiscale analysis of woven composite structures in MSC. Nastran. Adv Eng Softw 2019;135:102677.
[31] Long A, Brown L. Modelling the geometry of textile reinforcements for composites: TexGen. In: Composite reinforcements for optimum performance. Elsevier; 2011, p. 239–64.
[32] Mallikarachchi H, Pellegrino S. Quasi-static folding and deployment of ultrathin composite tape-spring hinges. J Spacecr Rockets 2011;48(1):187–98.
[33] Herath S, Jayasekara M, Mallikarachchi C. Parametric study on the homogenized response of woven carbon fibre composites. In: 2020 Moratuwa engineering research conference. IEEE; 2020, p. 36–41.
[34] Hamillage MY, Leung C, Kwok K. Viscoelastic modeling and characterization of thin-ply composite laminates. Compos Struct 2022;280:114901.
[35] Sankar BV, Marrey RV. Micromechanical models for textile composites. In: NASA, langley research center mechanics of textile composites conference. 1995.
[36] Xu W, Waas AM. A novel shell element for quasi-static and natural frequency analysis of textile composite structures. J Appl Mech 2014;81(8):081002.